

1 **Revision 2**

2  
3 **Comparative compressional behavior of chabazite with Li<sup>+</sup>, Na<sup>+</sup>, Ag<sup>+</sup>, K<sup>+</sup>,**  
4 **Rb<sup>+</sup>, and Cs<sup>+</sup> as extra-framework cations**

5 **by**

6 **Mihye Kong, Yongmoon Lee, G. Diego Gatta, Yongjae Lee**

7  
8 Corresponding author: **Yongjae Lee**, Department of Earth System sciences, Yonsei  
9 University, Seoul 03722, Republic of Korea - E-Mail: [yongjaelee@yonsei.ac.kr](mailto:yongjaelee@yonsei.ac.kr)

10  
11 *Manuscript submitted to The American Mineralogist for the special collection: "Microporous*  
12 *materials: crystal-chemistry, properties and utilizations"*

22 **Revision 2**

23  
24 **Comparative compressional behavior of chabazite with Li<sup>+</sup>, Na<sup>+</sup>, Ag<sup>+</sup>, K<sup>+</sup>,**  
25 **Rb<sup>+</sup>, and Cs<sup>+</sup> as extra-framework cations**

26  
27 **Mihye Kong<sup>1</sup>, Yongmoon Lee<sup>2</sup>, G. Diego Gatta<sup>3</sup>, Yongjae Lee<sup>1,2,\*</sup>**

28  
29 <sup>1</sup>Department of Earth System sciences, Yonsei University, Seoul 03722, Republic of Korea

30 <sup>2</sup>Center for High Pressure Science and Technology Advanced Research, Shanghai 201203,  
31 China

32 <sup>3</sup>Dipartimento di Scienze della Terra, Università degli Studi di Milano, Via Botticelli 23, I-  
33 20133 Milano, Italy

34  
35 **Abstract**

36 The high-pressure behavior of monovalent-cation-exchanged chabazites was  
37 investigated by means of *in-situ* synchrotron X-ray powder diffraction with a diamond anvil  
38 cell, and using water as penetrating pressure-transmitting medium, up to 5.5 GPa at room  
39 temperature. In all cases, except for Na-containing chabazites, a phase transition from the  
40 original rhombohedral ( $R\bar{3}m$ ) to triclinic symmetry (likely  $P\bar{1}$ ) was observed in the range  
41 between 3.0 GPa and 5.0 GPa. The phase transition is accompanied by an abrupt decrease of  
42 the unit-cell volume by up to 10 %. Evidence of pressure-induced hydration (PIH), i.e., *P*-  
43 induced penetration of H<sub>2</sub>O molecules through the zeolitic cavities, was observed, as  
44 reflected by the incompressibility of the cation-exchanged chabazites, which is governed by

45 the distribution of the extra-framework cations. The reversibility of the PIH and *P*-induced  
46 phase transitions in the high-pressure behavior of the cation-exchanged chabazites are  
47 discussed in the context of the role played by the chemical nature and bonding configuration  
48 of the extra-framework cations, along with that of the H<sub>2</sub>O content at room conditions.

49

50 **Keywords:** Chabazite, compressibility, high pressure, pressure-induced hydration,

51 synchrotron diffraction

52

53           **Introduction**

54           There is a growing interest in understanding the behavior of microporous materials at  
55 non-ambient conditions and, in particular, at high pressure (*e.g.*, Bish and Carey 2001; Alberti  
56 and Martucci 2005; Cruciani 2006; Gatta and Lee 2014; Gatta et al. 2017 and references  
57 therein). Pressure can cause important structural changes in microporous materials,  
58 modifying their physical-chemical properties and hence affecting their potential technological  
59 utilizations. Pressure-induced hydration (PIH) or pressure-induced insertion (PII), *i.e.*, *P*-  
60 induced penetration of external molecules through the zeolitic sub-nanocavities at moderate  
61 pressure ( $\leq 1$  GPa), is one of the most fascinating discovery in material science over the last  
62 decade, with potential technological and geological implications, recently reviewed by Gatta  
63 et al. (2017), promoting new routes for creating hybrid host-guest composite materials or for  
64 understanding the stability of clathrates or the role played by zeolites as carrier of H<sub>2</sub>O or  
65 CO<sub>2</sub> in subduction zones (*e.g.*, Lee et al. 2011; Seoung et al. 2013; Seoung et al. 2014;  
66 Seoung et al. 2015; Im et al. 2015). Framework topology and extra-framework content are the  
67 key factors that govern the structural deformations at high pressure (*e.g.*, Gatta et al. 2005;  
68 Gatta 2010; Danisi et al. 2015). Previous studies showed that the pressure-induced  
69 deformation of the tetrahedral framework in zeolites can be described in terms of tilting of  
70 quasi-rigid tetrahedra (*e.g.*, Gatta 2008; 2010; Gatta and Lee 2014). There has not, however,  
71 been any systematic study on how the framework distortion in response to the applied  
72 pressure is influenced by the nature and distribution of the extra-framework cations. Only the  
73 “fibrous zeolites group”, which was extensively investigated at high pressure, provided a  
74 preliminary model to describe the effect of the extra-framework population on the elastic  
75 behavior of isotypic materials (*e.g.*, Gatta 2005; Gatta et al. 2005; Seoung et al. 2013; Seoung  
76 et al. 2015).

77           Chabazite (ideally  $[(Ca_{0.5},K,Na)_x(H_2O)_{12}][Al_xSi_{12-x}O_{24}]$ , with  $x = 2.4 - 5.0$ ,  
78 <http://www.iza-online.org/natural/Datasheets/Chabazite/chabazite.htm>) is one of the most  
79 widespread natural zeolites with excellent ion-exchange properties (*e.g.*, Barrer et al. 1969;

80 Shang et al. 2012). Its framework is built up by double 6-membered rings (D6R), stacked in  
81 an ABC sequence and linked together through single 4-membered rings (S4R) (e.g.,  
82 Calligaris et al. 1982; Zema et al. 2008). As a result, the framework contains large ellipsoidal  
83 cavities (i.e., the CHA cage) with apertures of about  $6.7 \times 10 \text{ \AA}$ , which are accessible through  
84 single 8-rings (S8R) (Breck 1974). The largest opening of the S8R has a dimension of  $3.8 \times$   
85  $3.8 \text{ \AA}$  and is located in the direction normal to the (001) crystal plane (Smith et al. 2001;  
86 Shang et al. 2012). Chabazites crystallizes with rhombohedral symmetry (space group  $R\bar{3}m$ ),  
87 with only one independent tetrahedral framework site, populated by Al and Si with a  
88 statistically disordered distribution (Dent and Smith 1958). Exchangeable extra-framework  
89 cations and H<sub>2</sub>O molecules are distributed over the D6R, S8R, and CHA cages with various  
90 occupancies (e.g., Fialips et al. 2005). A recent structural study of our group on various  
91 monovalent cation-exchanged chabazites revealed the systematic interplay between the  
92 framework and the extra-framework cations, i.e., the unit-cell volume of monovalent-cation-  
93 exchanged chabazites varies in response to the ion selectivity, in the order of  $\text{Cs}^+ \geq \text{K}^+ > \text{Ag}^+$   
94  $> \text{Rb}^+ > \text{Na}^+ > \text{Li}^+$  (Kong et al. 2016).

95 The aim of this study is the description of the comparative compressional behavior  
96 of these monovalent cation-exchanged chabazites (Kong et al. 2016) and the potential crystal-  
97 fluid interactions in response to the applied hydrostatic pressure. We have performed *in-situ*  
98 high-pressure (at room temperature) synchrotron X-ray powder diffraction experiments on  
99 Li-, Na-, Ag-, K-, Rb-, and Cs-exchanged chabazites, using a diamond-anvil cell and pure  
100 water as a nominally pore-penetrating pressure-transmitting medium, in order to emulate the  
101 same conditions generated in industrial processes, or occurring in nature, in which water is  
102 the dominant *P*-fluid.

103

## 104 **Experimental methods**

105 A natural chabazite (hereafter ORI-CHA,  $\text{Ca}_{1.6}\text{Na}_{0.5}\text{Si}_{8.4}\text{Al}_{3.6}\text{O}_{24} \cdot 14.3\text{H}_2\text{O}$ , space

106 group  $R\bar{3}m$ ,  $a = 9.405(5)$  Å,  $\alpha = 94.22(2)^\circ$ ) from Rubendorf, Bohemia, was used in this  
107 study. Cation exchange was performed by stirring a mixture of ground ORI-CHA and the  
108 respective nitrate solution of Li, Na, Ag, K, Rb, and Cs, in a 1:100 weight ratio, in a closed  
109 system at 80°C for 72h. The final product was filtered, washed with distilled water, and air-  
110 dried. Elemental analysis (by X-ray fluorescence with energy-dispersive system detector)  
111 revealed that a complete ion-exchange was achieved, with the respective aforementioned  
112 cations. Further details pertaining to the ion-exchange protocols and crystallochemical  
113 characterization of the natural and final products are reported by Kong et al. (2016).

114 *In-situ* high-pressure (HP) synchrotron X-ray powder diffraction experiments on the  
115 as-prepared cation-forms of chabazites were performed at beamline 10-2 at the Stanford  
116 Synchrotron Radiation Lightsource (SSRL) at the SLAC National Accelerator Laboratory.  
117 At the beamline 10-2, the synchrotron radiation from the wiggler insertion device impinges  
118 on a Si(111) crystal followed by two pinholes in order to generate an approximately 200 µm  
119 diameter beam of monochromatic X-rays with a wavelength of 0.61992(5) Å. A Pilatus  
120 300K-w Si-diode CMOS detector, manufactured by DECTRIS, was used to collect the  
121 powder diffraction data. The detector, held at a distance of 1032(2) mm from the sample, was  
122 stepped to produce scattering angle coverage in  $2\theta$  up to ca. 40°. The position of the incident  
123 beam, sample to detector distance, and detector tilt were determined using LaB<sub>6</sub> (SRM 660)  
124 as a standard polycrystalline material.

125 A modified Merrill-Bassett diamond anvil cell (DAC), with two opposing diamonds  
126 supported by tungsten-carbide plates, was used for the high-pressure X-ray diffraction  
127 measurements. A stainless-steel foil of 250 µm thickness was pre-indented to a thickness of  
128 about 100 µm, and a 300 µm hole was obtained by electro-spark erosion. The powdered  
129 samples of Li-, Na-, Ag-, K-, Rb-, and Cs-exchanged chabazites were placed in the gasket  
130 hole together with a few ruby chips (~20 µm in diameter) for pressure measurements by the  
131 ruby-fluorescence method (following the protocol of Mao et al. 1986; error: ± 0.05 GPa).  
132 Ambient pressure data were collected first on the dry zeolite powder sample inside the DAC.

133 Subsequently, pure water was added into the gasket hole as a (hydrostatic, at  $P \leq 1$  GPa)  $P$ -  
134 transmitting medium (PTM), and the second ambient pressure data were collected using the  
135 ‘wet’ sample. The pressure was then increased and, at any pressure point, the sample was  
136 equilibrated for about 10 minutes before collecting the X-ray diffraction data. Water  
137 transforms to a solid phase at  $P \geq 1$  GPa (and room temperature), and the diffraction peaks of  
138 ice VI and VII were observed at pressure in excess of 1 GPa. The experiments were  
139 deliberately performed under non-hydrostatic conditions at  $P > 1$  GPa, in order to emulate the  
140 conditions of natural or industrial processes.

141 Pressure-dependent changes of the unit-cell lengths and volumes were derived from a  
142 series of Le Bail profile fittings (Le Bail et al. 1988) using the GSAS-EXPGUI suite of  
143 programs (Larson and Von Dreele 2004; Toby 2001). The background was fitted with a  
144 Chebyshev polynomial (with  $\leq 24$  coefficients), and the pseudo-Voigt profile function of  
145 Thompson et al. (1987) was used to model the Bragg peaks shape. Unfortunately, any attempt  
146 to perform Rietveld structure refinements (Rietveld 1969) was unsuccessful.

147 The (isothermal) bulk compressibility of the (low- $P$ ) rhombohedral polymorphs of  
148  $\text{Li}^+$ -,  $\text{Na}^+$ -,  $\text{Ag}^+$ -,  $\text{K}^+$ -,  $\text{Rb}^+$ - and  $\text{Cs}^+$ -chabazites is here described by the bulk modulus  $K_0$  ( $K_0 =$   
149  $1/\beta = -V \cdot \partial P / \partial V$ , where  $\beta$  is the isothermal compressibility coefficient), obtained by a second-  
150 order Birch-Murnaghan Equation of State (II-BM-EoS) fit (Birch 1947), using the EOS-fit  
151 V7.0 program (Angel et al. 2014) and the data weighted by the uncertainties in  $P$  and  $V$ .

152

## 153 **Results**

154 Synchrotron X-ray powder diffraction patterns collected at high pressure, using pure  
155 water as PTM, are shown in Fig. 1. A visual examination of the diffraction patterns reveals  
156 that, upon increasing pressure, the diffraction peaks exhibit gradual broadening. The  
157 broadening effect can be due to a number of factors, such as an increase in the long-range  
158 structural disorder and the growth of microstrains in response to the non-hydrostatic

159 conditions at  $P > 1$  GPa (*e.g.*, Yamanaka et al. 1997; Weidner et al. 1998; Fei and Wang 2000).  
160 Similar effects have been observed for the other isotypic CHA materials (*i.e.*, SAPO-34,  
161 ALPO-34) by Leardini et al. (2010, 2013). After pressure release back to ambient conditions,  
162 the peak positions, widths, and intensities revert back to those before compression, indicating  
163 the reversibility of the  $P$ -induced deformation mechanisms in all the cation-exchanged  
164 chabazites within the  $P$ -range investigated (Fig. 1). At  $P > 3$  GPa, phase transitions from  
165 rhombohedral to triclinic symmetry are observed in chabazites exchanged with  $\text{Li}^+$ ,  $\text{K}^+$ ,  $\text{Ag}^+$ ,  
166  $\text{Rb}^+$  and  $\text{Cs}^+$ , whereas the natural chabazite and the Na-form do not experience any transition  
167 (Figs. 1 and 2 and Table 1). These phase transitions are driven by an abrupt decrease of the  
168 unit-cell volume in the range between 2.0 and 10 % (Fig. 2).

169 The compressional pattern of the natural chabazite (ORI-CHA,  
170  $\text{Ca}_{1.6}\text{Na}_{0.5}\text{Si}_{8.4}\text{Al}_{3.6}\text{O}_{24}\cdot 14.3\text{H}_2\text{O}$ ) in water PTM shows a monotonic trend, though with a  
171 softening which is more pronounced at  $P > 2$  GPa (Figs. 1 and 2, Table 1). The refined bulk  
172 modulus (deduced on the basis of the low- $P$  data pre-softening) is  $K_0(\text{ORI-CHA}) = 88(3)$   
173 GPa, while the measured unit-cell volume at ambient pressure is  $V_0(\text{ORI-CHA}) = 824.9(9)$   
174  $\text{\AA}^3$ .

175 When Li-CHA ( $\text{Li}_{1.9}\text{Si}_{8.6}\text{Al}_{3.4}\text{O}_{24}\cdot 13.2\text{H}_2\text{O}$ ) is compressed in water PTM from  $P_{\text{amb}}$  to  
176 5.5 GPa, the unit-cell volume decreases steadily below 3.0 GPa. Above this pressure, the  
177 rhombohedral structure transforms into a triclinic one (Figs. 1 and 2, Table 1), accompanied  
178 by abrupt and anisotropic contraction of the unit-cell edges by ca. 0.8 %, 2.0 %, and 4.5 % for  
179 the  $a$ -,  $b$ -, and  $c$ -edge lengths, respectively, of the high- $P$  triclinic polymorph (Fig. 2). This  
180 leads to an overall volume reduction by ca. 3.0 %. Bulk modulus at ambient pressure,  
181 calculated for the low- $P$  rhombohedral polymorph of Li-CHA, is  $K_0(\text{Li-CHA}) = 202(2)$  GPa  
182 with the measured  $V_0(\text{Li-CHA})$  of  $819.9(9) \text{\AA}^3$ . The bulk modulus of Li-CHA is the highest  
183 amongst the studied cation-exchanged chabazites (hence with the lowest compressibility),  
184 whereas its volume at ambient pressure is the smallest.



185 In the case of Na-CHA ( $\text{Na}_{3.4}\text{Si}_{8.6}\text{Al}_{3.4}\text{O}_{24}\cdot 11.4\text{H}_2\text{O}$ ), compression in water PTM up  
186 to 5.3 GPa leads to a steady decrease of unit-cell volume without phase transition, though  
187 with a modest volume expansion at very low- $P$  (0.5 GPa, Table 1) and softening at  $P > 2$  GPa  
188 (Figs. 1 and 2, Table 1). The refined bulk modulus at ambient pressure (deduced on the basis  
189 of the low- $P$  data pre-softening) is  $K_0(\text{Na-CHA}) = 114(9)$  GPa with the measured  $V_0$  (Na-  
190 CHA) of  $824.9(9) \text{ \AA}^3$ .

191 In Ag-CHA ( $\text{Ag}_{3.5}\text{Si}_{8.5}\text{Al}_{3.5}\text{O}_{24}\cdot 15.9\text{H}_2\text{O}$ ), the steady initial contraction of the unit-cell  
192 edges in water PTM is followed by a transition to a triclinic structure above ca. 5.7 GPa,  
193 accompanying abrupt and anisotropic contractions of the  $a$ -,  $b$ -, and  $c$ -edge lengths, of the  
194 triclinic polymorph, by ca. 0.4 %, 3.3 %, and 8.7 %, respectively (Figs. 1 and 2, Table 1).  
195 This leads to an overall volume reduction by ca. 10.0 %. The refined bulk modulus at  
196 ambient pressure, calculated for the low- $P$  rhombohedral polymorph of Ag-CHA, is  $K_0(\text{Ag-}$   
197 CHA) =  $116(2)$  GPa with the measured  $V_0$  (Ag-CHA) of  $829.2(2) \text{ \AA}^3$ .

198 Similar transition from rhombohedral to triclinic structure is observed in K-CHA  
199 ( $\text{K}_{3.2}\text{Si}_{8.7}\text{Al}_{3.3}\text{O}_{24}\cdot 10.7\text{H}_2\text{O}$ ) compressed in water at ca. 5.1 GPa (Figs. 1 and 2, Table 1). Also  
200 in this case, the transition is accompanied by abrupt and anisotropic contraction of the unit-  
201 cell edges by ca. 1.5 %, 1.5 %, and 6.5 % for the  $a$ -,  $b$ -, and  $c$ -edge lengths, respectively (Fig.  
202 2), which leads to an overall volume reduction of the high- $P$  triclinic polymorph by ca. 6.0 %.  
203 The refined bulk modulus of the low- $P$  rhombohedral polymorph of K-CHA is  $K_0(\text{K-CHA}) =$   
204  $93(1)$  GPa, the lowest value amongst the ion-exchanged chabazites of this study, whereas the  
205 measured unit-cell volume at ambient pressure is  $V_0(\text{K-CHA}) = 830.8(8) \text{ \AA}^3$ .

206 Compression of Rb-CHA ( $\text{Rb}_{4.1}\text{Si}_{7.9}\text{Al}_{4.1}\text{O}_{24}\cdot 6.5\text{H}_2\text{O}$ ) in water PTM to 6.0 GPa shows  
207 a modest volume expansion at very low- $P$  (0.5 GPa, Table 1) and then a gradual monotonic  
208 decrease of the unit-cell volume up to ca. 4.9 GPa, followed by abrupt contraction by ca. 5.0 %  
209 in response to the rhombohedral-to-triclinic phase transition (Figs. 1 and 2, Table 1). This  
210 transition is also driven by anisotropic contraction of the unit-cell edges, of the triclinic

211 polymorph, by ca. 1.9 %, 0.7 %, and 4.8 % for the *a*-, *b*-, and *c*-edge lengths, respectively  
212 (Fig. 2). The refined bulk modulus of low-*P* rhombohedral Rb-CHA is the second largest  
213 after Li-CHA:  $K_0(\text{Rb-CHA}) = 149(5)$  GPa, with a measured  $V_0(\text{Rb-CHA}) = 826.0(1)$  Å<sup>3</sup>.

214 For Cs-CHA ( $\text{Cs}_{3.4}\text{Si}_{8.6}\text{Al}_{3.4}\text{O}_{24}\cdot 6.4\text{H}_2\text{O}$ ), a modest volume expansion at very low-*P*  
215 (0.5 GPa, Table 1) followed by a monotonic compression is also observed (Figs. 1 and 2,  
216 Table 1). The degree of volume contraction during the rhombohedral-to-triclinic transition,  
217 between 3 and 4 GPa, is modulated to ca. 2.0% with anisotropic reduction of the unit-cell  
218 edges by ca. 1.4 %, 1.2 %, and 1.1 % for the *a*-, *b*-, and *c*-edges lengths, respectively, of the  
219 triclinic form (Figs. 1 and 2, Table 1). Bulk modulus and (measured) unit-cell volume at  
220 ambient pressure for the low-*P* rhombohedral polymorph are:  $K_0(\text{Cs-CHA}) = 137(1)$  GPa  
221 and  $V_0(\text{Cs-CHA}) = 830.4(4)$  Å<sup>3</sup>, respectively.

222

## 223 Discussion and Implications

224 The experimental findings of this study, in which a nominally penetrating *P*-  
225 transmitting fluid is used (*sensu* Gatta 2008), allow first of all a comparison between the  
226 compressional behavior of a natural chabazite in penetrating and non-penetrating media.  
227 Leardini et al. (2010, 2013) reported the behavior of two natural chabazites, with slightly  
228 different compositions, compressed in silicone oil (a non-penetrating *P*-medium) and showed:  
229 a change of the compressional behavior at 1.4 GPa in one of the samples, with chemical  
230 formula  $(\text{K}_{1.36}\text{Ca}_{1.04}\text{Na}_{0.28}\text{Sr}_{0.4}\text{Ba}_{0.06}\text{Mg}_{0.02})[\text{Si}_{7.17}\text{Al}_{4.87}\text{O}_{24}]\cdot 13.16\text{H}_2\text{O}$ , with an estimated bulk  
231 modulus of 35(5) GPa at  $P < 1.4$  GPa and 62(1) at  $P > 1.4$  GPa (Leardini et al. 2010); a  
232 rhombohedral-to-triclinic phase transition at 2.1 GPa in the second chabazite sample, with  
233 chemical formula  $(\text{Ca}_{1.32}\text{K}_{0.45}\text{Na}_{0.13}\text{Sr}_{0.10})[\text{Si}_{8.55}\text{Al}_{3.45}\text{O}_{24}]\cdot 11.30\text{H}_2\text{O}$ , with an estimated bulk  
234 modulus of 54(3) GPa for the low-*P* polymorph. Further *HP*-experiments on the synthetic  
235 ALPO-34 and SAPO-34, isotypic materials with CHA framework topology, were performed  
236 using non-penetrating fluids: the bulk modulus of the ALPO-34 was reported to be 54(3)

237 (Leardini et al. 2012) and that of SAPO-34 of 29(1) GPa (Leardini et al. 2010). While ALPO-  
238 34 is free of extra-framework cations, SAPO-34 contains organic template and water  
239 molecules in the CHA cages. If we consider all the data available in the open literature, the  
240 “expected” bulk modulus (at room conditions) of a natural (rhombohedral) chabazite is  
241  $50\pm 15$  GPa. In our study, the bulk modulus of the natural chabazite compressed in water, a  
242 nominally penetrating fluid, leads to a bulk modulus of about 90 GPa. This value is, in  
243 general, unusual for zeolites (*i.e.*, too high, Gatta and Lee 2014) and, in this specific case,  
244 suggests that the H<sub>2</sub>O molecules penetrate through the zeolitic cavities in response to the  
245 applied pressure. The continuous penetration of the extra H<sub>2</sub>O molecules would lead to more  
246 efficient stuffing of the pores by extra-framework species, making the zeolite structure less  
247 compressible. This can explain the higher bulk modulus observed in this study if compared to  
248 those obtained in previous experiments with non-penetrating *P*-fluids, in which the inherent  
249 compressibility is obtained. A similar effect was previously observed in several HP-  
250 experiments on zeolites (compressed in penetrating and non-penetrating fluids) and provides  
251 “indirect” evidence of PIH in our experiment, useful when “direct” evidence are missed due  
252 to the lack of abrupt structural changes and/or structural models (*i.e.*, impossibility to perform  
253 Rietveld structure refinements).

254         Without data at atomic scale obtained by structure refinements, it is not certain if the  
255 penetration of extra H<sub>2</sub>O molecules occurs entirely at very low-*P* ( $\leq 0.5$  GPa), as suggested  
256 by the modest volume expansion in Na-, Rb- and Cs-CHA (Table 1) and as observed for  
257 several zeolites (Gatta 2008; Gatta and Lee 2014 and references therein), or it is a continuous  
258 process within the *P*-range investigated. In the second case, the bulk modulus value does not  
259 have a robust physical meaning, because the composition of the zeolite changes with  
260 increasing pressure (*i.e.*, the system is “open”). However, the “apparent” compressibility,  
261 through the bulk modulus, remains a useful measure for a comparative analysis (*e.g.*, the  
262 same zeolite compressed in different fluids; zeolites with the same framework topology and  
263 different extra-framework population compressed in the same fluid).

264 The compressional behavior of all the cation-exchanged chabazites of this study allow us  
265 to make the following observations and considerations:

266 1) Our results indicate an inverse relationship between the onset pressure of the  
267 rhombohedral-to-triclinic transition and the radius of extra-framework cation in  
268 chabazite, above the ca. 1.0 Å threshold (Fig. 3). Similar trend is observed between  
269 the degree of volume contraction and the radius of extra-framework cation, which  
270 appears to be mainly driven by the *c*-edge length contraction of the triclinic  
271 polymorph (Fig. 3, Table 1). The largest contraction along the *c*-axis is ca. 8.7% in  
272 Ag-CHA, whereas in K-CHA, Rb-CHA, and Cs-CHA, the contractions are by ca. 6.5,  
273 4.8, and 1.4%, respectively (Fig. 3). The different volume contraction, in response to  
274 the phase transition, might be partly related to the initial H<sub>2</sub>O content at ambient  
275 conditions. In Ag-CHA there are ca. 15.9 H<sub>2</sub>O molecules per formula unit (p.f.u.),  
276 which decrease to ca. 10.7, 6.5, and 6.4 in K-CHA, Rb-CHA, and Cs-CHA,  
277 respectively (Fig. 3). On the other hand, there are ca. 13.2 H<sub>2</sub>O p.f.u. in Li-CHA,  
278 which exhibits lower transition pressure and volume contraction than Ag-CHA (Fig.  
279 3): Li-CHA appears to be an outlier in the contraction vs. cation radius relationship  
280 and needs further structural investigation.

281 2) There is an additional experimental finding about a potential relation between the  
282 observed bulk modulus and the distribution of extra-framework cations over the  
283 different segments forming the chabazite cavities, *i.e.*, D6R, S8R, and CHA-cage (Fig.  
284 4). The highest bulk modulus of 202(2) GPa is observed for the rhombohedral low-*P*  
285 polymorph of Li-CHA, where Li-cations fill all the three cavities (D6R, S8R, and  
286 CHA-cage) at ambient conditions. More compressible than Li-CHA are Rb-CHA and  
287 Cs-CHA with bulk moduli of 149(5) and 137(1) GPa, respectively. In these chabazites,  
288 the extra-framework cations populate the S8R and CHA-cages only (*i.e.*, no D6R).  
289 The most compressible forms are then Ag-CHA, Na-CHA, and K-CHA with bulk  
290 moduli of 116(2), 114(9), and 93(1) GPa, respectively. In these compounds, extra-

291 framework cations are only located in the largest CHA-cages (*i.e.*, no D6R or S8R).  
292 3) All the high-*P* deformation mechanisms and penetration phenomena are reversible, as  
293 proved by the diffraction data collected at room conditions after decompression (Fig.  
294 1, Table 1).

295 Overall, it appears that:

296 1) PIH occurs in the natural and in all the cation-exchanged chabazites of this study, and  
297 it is reversible. This is true even in the case of Na-CHA, which does not experience  
298 any *P*-induced phase transition but reacts, in response to the applied pressure, with a  
299 bulk modulus of 114(9) GPa, not realistic for a zeolite without any crystal-fluid  
300 interaction (Gatta 2008, Gatta and Lee 2014). At this stage, it is unknown why the  
301 ORI-CHA and Na-CHA do not experience the *P*-induced phase transition observed  
302 for the other cation-exchanged forms of this study. Likely, the higher number of  
303 independent extra-framework sites in these two chabazites (*i.e.*, ORI-CHA: 4Ca +  
304 3Na + 5OW; Na-CHA: 4Na + 7OW; Li-CHA: 4Li + 5OW; K-CHA: 3K + 5OW; Rb-  
305 CHA: 2Rb + 2OW; Cs-CHA: 2Cs + 2OW; Ag-CHA: 2Ag + 2OW; Kong et al. 2016)  
306 makes their structures more “flexible”, with higher degrees of freedom  
307 accommodating the *P*-induced deformation effects.

308 2) The degree of PIH is somewhat controlled by the distribution of the extra-framework  
309 cations (which, in turn, reflects their ionic radius and charge) and how these can  
310 coordinate extra H<sub>2</sub>O molecules. Li, for example, is a small ion and its coordination  
311 polyhedra leaves room in the cavities for additional H<sub>2</sub>O molecules, which can be  
312 further coordinated by Li or can be H-bonded to the framework oxygens. However,  
313 the different number (and location inside the cavities) of independent cation sites and  
314 H<sub>2</sub>O molecules in the cation-exchanged chabazites of this study does not allow to  
315 define a universal and unambiguous model to explain the behavior of all the cation-  
316 exchanged chabazites.

317

318 We can draw geological implications of our experimental findings as follows. Our  
319 results demonstrate that small molecules (in kinetic diameters), like H<sub>2</sub>O, CO<sub>2</sub>, CH<sub>4</sub> or H<sub>2</sub>S,  
320 can potentially penetrate into the CHA-type zeolites in response to the applied pressure. Such  
321 a penetration phenomenon is likely to be active even at very low pressures (kilobar level or  
322 even lower). Geological fluids can, therefore, interact efficiently with this zeolite with a  
323 significant fluid-to-crystal mass transfer. In other words, the ability of zeolites, as  
324 microporous materials, to act as geochemical traps of small molecules can be drastically  
325 enhanced at moderate pressures even at room temperature; it is highly likely that the  
326 combined effect of pressure and temperature would improve the magnitude of the PIH and  
327 PII, as previously observed in other zeolites (Gatta and Lee 2014 and references therein).

328 The technological implications of our results are even more relevant. Our  
329 experimental findings demonstrate that it is possible to modulate the elastic behavior of a  
330 given zeolite simply by cation-exchange and using a penetrating *P*-transmitting fluid. A  
331 combined [A<sup>+</sup>-CHA + H<sub>2</sub>O] system (with A<sup>+</sup> = Li, Na, Ag, K, Rb, Cs) can behave like a low-  
332 compressibility “spring”: the bulk modulus of the Li-CHA in H<sub>2</sub>O (*i.e.*, 202(2) GPa) is higher,  
333 in certain *P*-range, than those of garnets (~190 GPa, Hazen et al. 1994), mullites (~ 170 GPa,  
334 Gatta et al. 2010, 2013) or topaz (~160 GPa, Gatta et al. 2006, 2014). With different cations,  
335 it is possible to generate hybrid softer systems with modulated bulk moduli targeting certain  
336 solids such as olivines (~ 120-130 GPa, Smyth et al. 2000), pyroxenes (~ 90-130 GPa,  
337 McCarthy et al. 2008) or feldspars (~ 50-80 GPa, Angel 2004). This is surprising if we  
338 consider that zeolites are microporous materials and intuitively considered as soft compounds.  
339 PIH observed in this study for the natural and for all the cation-exchanged chabazites, is a  
340 reversible phenomenon and cannot be used to generate super-hydrated zeolites which remain  
341 metastable at room conditions after decompression. However, it would be different for other  
342 small molecules and/or mixed cation chabazites. In this light, further studies are in progress  
343 in order to expand the number of small molecules able to penetrate the CHA-cavities at high  
344 pressure.

345 **Acknowledgments**

346 This work was supported by the Global Research Laboratory (NRF-2009-00408) and  
347 National Research Laboratory (NRF-2015R1A2A1A01007227) programs of the Korean  
348 Ministry of Science, ICT and Planning (MSIP). We also thank the supports by NRF-  
349 2016K1A4A3914691 and NRF-2016K1A3A7A09005244 grants. Experiments using X-ray  
350 synchrotron radiation were supported by the Collaborative Access Program of SSRL.

351           **References**

352           Alberti, A. and Martucci, A. (2005) Phase transformations and structural  
353 modifications induced by heating in microporous materials. *Studies in surface science and*  
354 *catalysis*, 155, 19-43.

355           Angel, R.J. (2004) Equations of state of plagioclase feldspars. *Contributions to*  
356 *Mineralogy and Petrology*, 146, 506–512.

357           Angel, R.J., Gonzalez-Platas, J., and Alvaro, M. (2014) EosFit-7c and a fortran  
358 module (library) for equation of state calculations. *Zeitschrift für Kristallographie*, 229, 405-  
359 419.

360           Barrer, R.M., Davies, J.A., and Rees, L.V.C. (1969) Thermodynamics and  
361 thermochemistry of cation exchange in chabazite. *Journal of Nuclide Chemistry*, 31, 219-232.

362           Bish, D.L. and Carey, J.W. (2001) Thermal behavior of natural zeolites. *Reviews in*  
363 *Mineralogy and Geochemistry*, 45, 403–452.

364           Birch, F. (1947) Finite elastic strain of cubic crystals. *Physical Review*, 71, 809-824.

365           Breck, D.W. (1974) *Zeolite molecular sieves: Structure, chemistry and use*. Wiley  
366 and Sons, New York (original edition); reprinted R.E. Krieger, F.L. Malabar, 1984 (new  
367 edition).

368           Calligaris, M., Nardin, G., and Randaccio, L. (1982) Cation-site location in a natural  
369 chabazite. *Acta Crystallographica*, B38, 602-605.

370           Cruciani, G. (2006) Zeolites upon heating: Factors governing their thermal stability  
371 and structural changes. *Journal of Physics and Chemistry of Solids*, 67, 1913-2240.

372           Danisi, R.M., Armbruster, T., Arletti, R., Gatta, G.D., Vezzalini, G., Quartieri, S., and  
373 Dmitriev, V. (2015) Elastic behavior and pressure-induced structural modifications of the  
374 microporous Ca(VO)Si<sub>4</sub>O<sub>10</sub>·4H<sub>2</sub>O dimorphs cavansite and pentagonite. *Microporous and*



375 Mesoporous Materials, 204, 257-268.

376 Dent, L.S. and Smith, J.V. (1958) Crystal structure of chabazite, a molecular sieve.  
377 Nature, 181, 1794-1796.

378 Fei, Y. and Wang, Y. (2000) High-pressure and high-temperature powder diffraction.  
379 Reviews in Mineralogy and Geochemistry, 41, 521-557.

380 Fialips, C.I., Carey, J.W., and Bish, D.L. (2005) Hydration-dehydration behavior and  
381 thermodynamics of chabazite. Geochimica et Cosmochimica Acta, 69, 2293-2308.

382 Gatta, G.D. (2005) A comparative study of fibrous zeolites under pressure. European  
383 Journal of Mineralogy, 17, 411-421.

384 Gatta, G.D. (2008) Does porous mean soft? On the elastic behavior and structural  
385 evolution of zeolites under pressure. Zeitschrift für Kristallographie, 223, 160-170.

386 Gatta, G.D. (2010) Extreme deformation mechanisms in open-framework silicates at  
387 high-pressure: Evidence of anomalous inter-tetrahedral angles. Microporous and Mesoporous  
388 Materials, 128, 78-84.

389 Gatta, G.D. and Lee, Y. (2014) Zeolites at high pressure: A review. Mineralogical  
390 Magazine, 78, 267-291.

391 Gatta, G.D., Boffa Ballaran, T., Comodi, P., and Zanazzi, P.F. (2004) Comparative  
392 compressibility and equation of state of orthorhombic and tetragonal edingtonite. Physics and  
393 Chemistry of Minerals, 31, 288-298.

394 Gatta, G.D., Nestola, F., and Boffa Ballaran, T. (2006) Elastic behaviour and  
395 structural evolution of topaz at high pressure. Physics and Chemistry of Minerals, 33, 235-  
396 242.

397 Gatta, G.D., Rotiroti, N., Fisch, M., and Armbruster, T. (2010) Stability at high  
398 pressure, elastic behavior and pressure-induced structural evolution of “Al<sub>5</sub>BO<sub>9</sub>”, a mullite-

399 type ceramic material. *Physics and Chemistry of Minerals*, 37, 227-236.

400 Gatta, G.D., Lotti, P., Merlini, M., Liermann, H.-P., and Fisch, M. (2013) High-  
401 pressure behavior and phase stability of  $\text{Al}_5\text{BO}_9$ , a mullite-type ceramic material. *Journal of*  
402 *the American Ceramic Society*, 96, 2583–2592.

403 Gatta, G.D., Morgenroth, W., Dera, P., Petitgirard, S., and Liermann, H-P. (2014)  
404 Elastic behavior and pressure-induced structure evolution of topaz up to 45 GPa. *Physics and*  
405 *Chemistry of Minerals*, 41, 569-577.

406 Gatta, G.D., Lotti, P., and Tabacchi, G. (2017) The effect of pressure on open-  
407 framework silicates: elastic behaviour and crystal–fluid interaction. *Physics and Chemistry of*  
408 *Minerals* (in press, DOI: 10.1007/s00269-017-0916-z).

409 Hazen, R.M., Downs, R.T., Conrad, P.G., Finger, L.W., and Gasparik, T. (1994)  
410 Comparative compressibilities of majorite-type garnets. *Physics and Chemistry of Minerals*,  
411 21, 344–349.

412 Im, J., Seoung, D., Lee, S.Y., Blom, D.A., Vogt, T., Kao, C.-C., and Lee, Y. (2015)  
413 Pressure-Induced Metathesis Reaction To Sequester Cs. *Environmental Science and*  
414 *Technology*, 49, 513-519.

415 Kong, M., Liu, Z., Vogt, T., and Lee, Y. (2016) Chabazite structures with  $\text{Li}^+$ ,  $\text{Na}^+$ ,  
416  $\text{Ag}^+$ ,  $\text{K}^+$ ,  $\text{NH}_4^+$ ,  $\text{Rb}^+$  and  $\text{Cs}^+$  as extra-framework cations. *Microporous and Mesoporous*  
417 *Materials*, 221, 253-263.

418 Larson, A.C. and Von Dreele, R.B. (2004) General structure analysis system (GSAS),  
419 Los Alamos National Laboratory Report LAUR 86–748.

420 Leardini, L., Quartieri, S., and Vezzalini, G. (2010) Compressibility of microporous  
421 materials with CHA topology: 1. Natural chabazite and SAPO-34. *Microporous and*  
422 *Mesoporous Materials*, 127, 219-227.

423 Leardini, L., Quartieri, S., Martucci, A., Vezzalini, M.G., Dmitriev, V. (2012)  
424 Compressibility of microporous materials with CHA topology: 2. ALPO-34. Zeitschrift fuer  
425 Kristallographie, 227, 514-521.

426 Leardini, L., Quartieri, S., Vezzalini, G., Martucci, A., and Dmitriev, V. (2013)  
427 Elastic behavior and high pressure-induced phase transition in chabazite: New data from a  
428 natural sample from Nova Scotia. Microporous and Mesoporous Materials, 170, 52-61.

429 Le Bail, A., Duroy, H., and Fourquet, J.L. (1988) Ab-initio structure determination of  
430  $\text{LiSbWO}_6$  by X-ray powder diffraction. Materials Research Bulletin, 23, 447–452.

431 Lee, Y., Liu, D., Seoung, D., Liu, Z., Kao, C.-C., and Vogt, T. (2011) Pressure- and  
432 Heat-Induced Insertion of  $\text{CO}_2$  into an Auxetic Small-Pore Zeolite. Journal of the American  
433 Chemical Society, 133, 1674-1677.

434 Mao, H.K., Xu, J., and Bell, P.M. (1986) Calibration of the ruby pressure gauge to  
435 800 kbar under quasi-hydrostatic conditions. Journal of Geophysical Research, 91, 4673–  
436 4676.

437 McCarthy, A.C., Downs, R.T., and Thompson, R.M. (2008) Compressibility trends of  
438 the clinopyroxenes, and in-situ high-pressure single-crystal X-ray diffraction study of jadeite.  
439 American Mineralogist, 93, 198–209.

440 Seoung, D., Lee, Y., Kao, C.-C., Vogt, T., and Lee, Y. (2013) Super-Hydrated Zeolites:  
441 Pressure-Induced Hydration in Natrolites. Chemistry - A European Journal, 19, 10876–10883.

442 Seoung, D., Lee, Y., Cynn, H., Park, C., Choi, K.-Y., Blom, D.A., Evans, W.J., Kao,  
443 C.-C., Vogt, T., and Lee, Y. (2014) Irreversible Xenon Insertion into a Small Pore Zeolite at  
444 Moderate Pressures and Temperatures. Nature Chemistry, 6, 835-839.

445 Seoung, D., Lee, Y., Kao, C.-C., Vogt, T., and Lee, Y. (2015) Two-Step Pressure-  
446 Induced Superhydration in Small Pore Natrolite with Divalent Extra-Framework Cations.  
447 Chemistry of Materials, 27, 3874-3880.

448 Shang, J., Li, G., Singh, R., Gu, Q., Nairn, K.M., Bastow, T.J., Medhekar, N.,  
449 Doherty, C.M., Hill, A.J., Liu, J.Z., and Webley, P.A. (2012) Discriminative Separation of  
450 Gases by a “Molecular Trapdoor” Mechanism in Chabazite Zeolites. *Journal of the American*  
451 *Chemical Society*, 134, 19246-19253.

452 Smith, L.J., Eckert, H., and Cheetham, A.K. (2001) Potassium cation effects on site  
453 preferences in the mixed cation zeolite Li, Na-chabazite. *Chemistry of Materials*, 13, 385-391.

454 Smyth, J.R., Jacobsen, S.D., and Hazen, R.M. (2000) Comparative crystal chemistry  
455 of orthosilicate minerals. *Reviews in Mineralogy and Geochemistry*, 41, 187-209.

456 Thompson, P., Cox, D.E., and Hastings, J.B. (1987) Rietveld refinement of Debye-  
457 Scherrer synchrotron X-ray data from Al<sub>2</sub>O<sub>3</sub>. *Journal of Applied Crystallography*, 20, 79-83.

458 Toby, B.H. (2001) EXPGUI, a graphical user interface for GSAS. *Journal of Applied*  
459 *Crystallography*, 34, 210-213.

460 Rietveld, H.M. (1969) A profile refinement method for nuclear and magnetic  
461 structures. *Journal of Applied Crystallography*, 2, 65–71.

462 Weidner, D.J., Wang, Y.B., Chen, G., Ando, J., and Vaughan, M.T. (1998) Rheology  
463 measurements at high pressure and temperature. In M.H. Manghnani and T. Yagi, Eds.,  
464 *Properties of Earth and Planetary Materials at High Pressure and Temperature. Geophysical*  
465 *Monograph. American Geophysical Union, Washington, DC, p. 473–480.*

466 Yamanaka, T., Nagai, T., and Tsuchiya, T. (1997) Mechanism of pressure-induced  
467 amorphization. *Zeitschrift für Kristallographie*, 212, 401-410.

468 Zema, M., Tarantino, S.C., and Montagna, G. (2008) Hydration/Dehydration and  
469 cation migration processes at high temperature in zeolite chabazite. *Chemistry of Materials*,  
470 20, 5876-5887.

471

472

473 **Figure captions**

474 Figure 1. Synchrotron X-ray powder diffraction patterns as a function of hydrostatic  
475 pressure mediated by pure water as *P*-transmitting medium for (a) ORI-CHA, (b) Li-CHA, (c)  
476 Na-CHA, (d) Ag-CHA, (e) K-CHA, (f) Rb-CHA, and (g) Cs-CHA. Some of the new peak  
477 positions due to symmetry lowering are indicated with Miller indices.

478

479 Figure 2. Evolution of the unit-cell edges lengths (Å) and volume (Å<sup>3</sup>) with *P*, using pure  
480 water as *P*-transmitting medium, for (a) ORI-CHA, (b) Li-CHA, (c) Na-CHA, (d) Ag-CHA,  
481 (e) K-CHA, (f) Rb-CHA, and (g) Cs-CHA. The errors associated with the cell parameters are  
482 smaller than the symbols. The dashed lines represent only a guide for eyes. For the unit-cell  
483 volume, the red symbols indicate the triclinic high-*P* polymorphs.

484

485 Figure 3. Changes in the (a) unit-cell volume, (b) *c*-edge length, and (c) onset pressure of  
486 the rhombohedral-to-triclinic transition as a function of the ionic radius of the extra-  
487 framework cation in the alkali-metal-exchanged chabazites.

488

489 Figure 4. (a) Site distribution and (b) occupancy of the extra-framework cations, and (c)  
490 initial H<sub>2</sub>O molecular contents per formula unit in the alkali-metal-exchanged chabazites at  
491 ambient conditions. (d) “Observed” bulk moduli plotted as a function of cation radius.

492

493

494

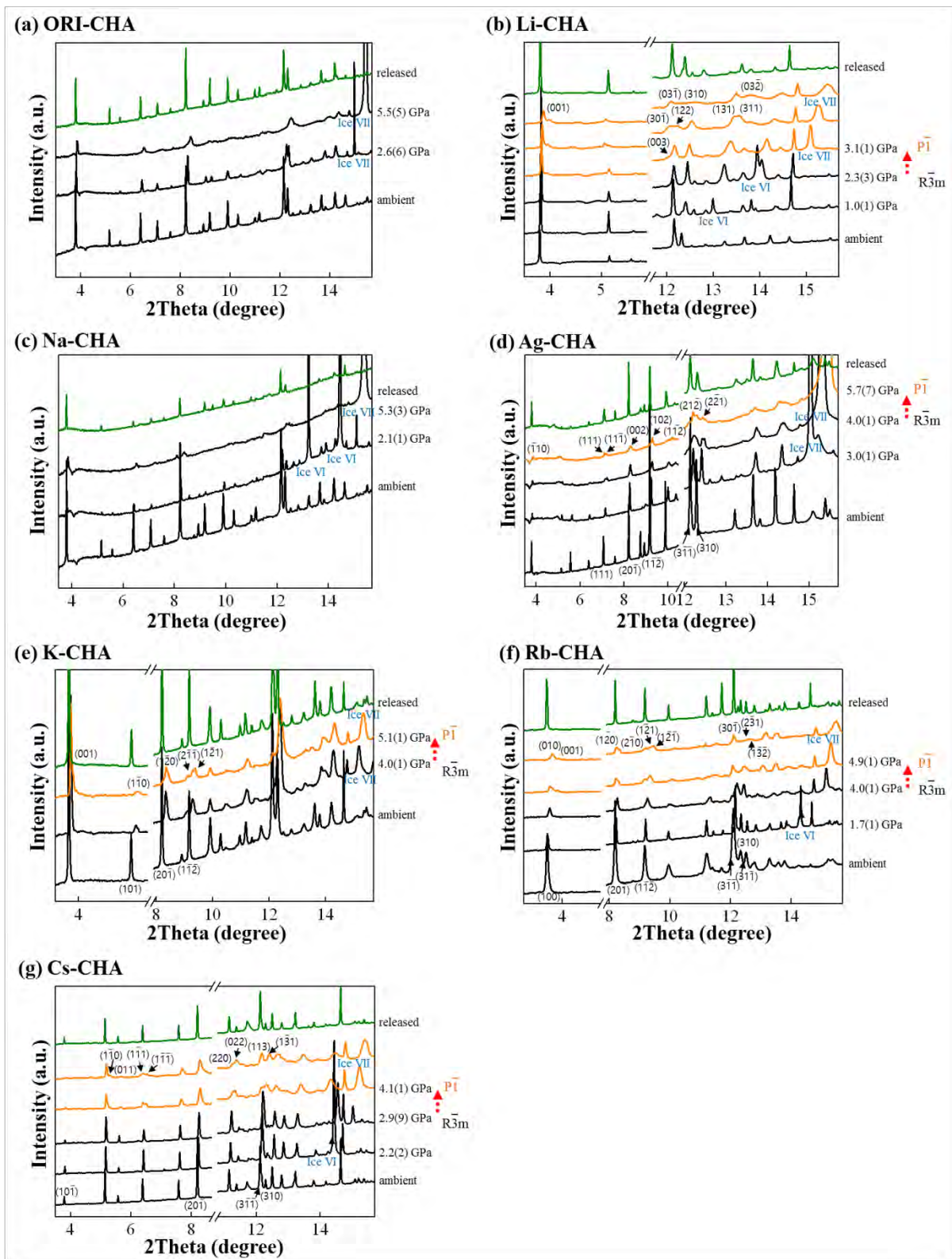
495

496

497

498

499 Figure 1.

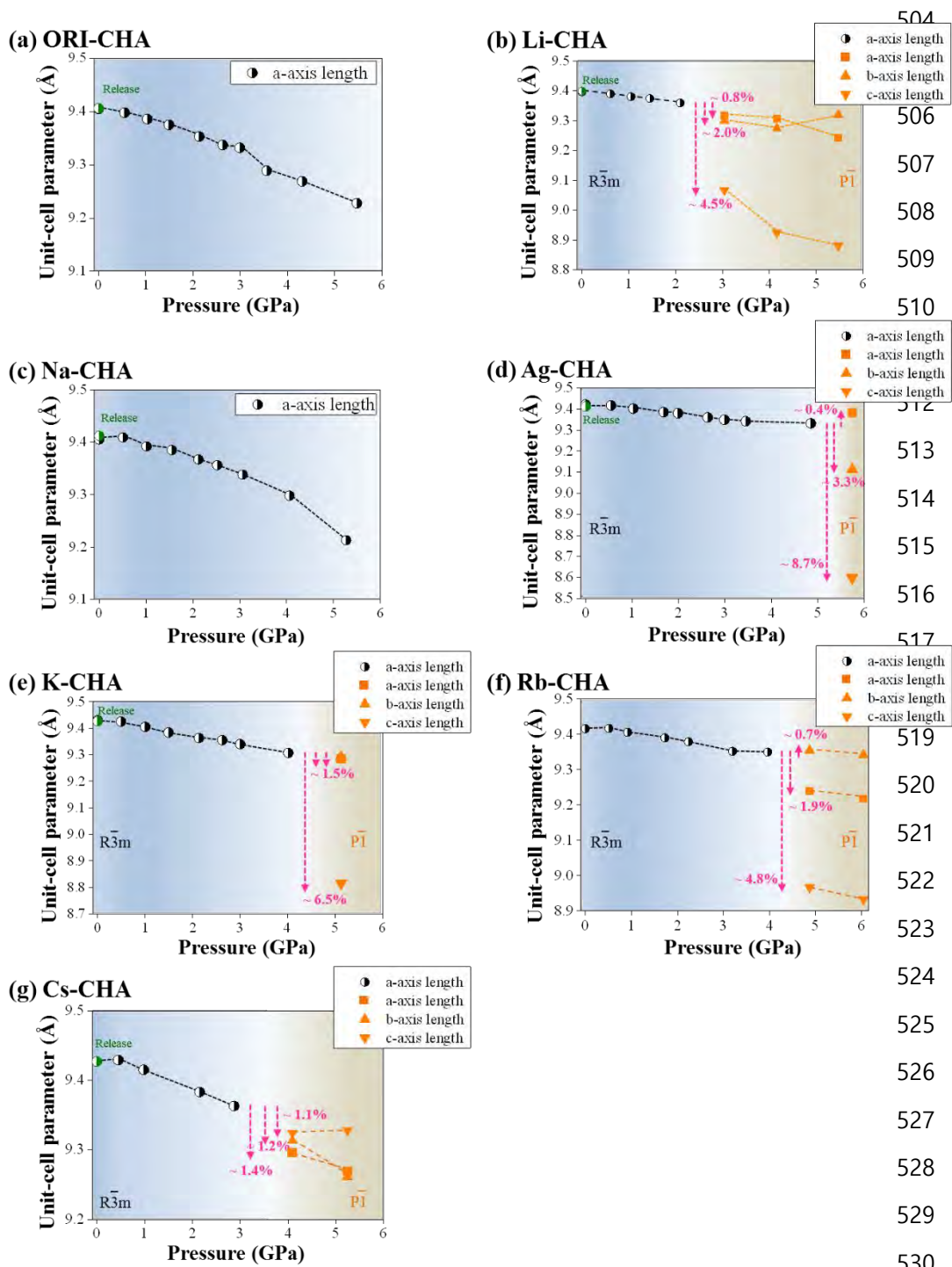


500

501

502

503 Figure 2.



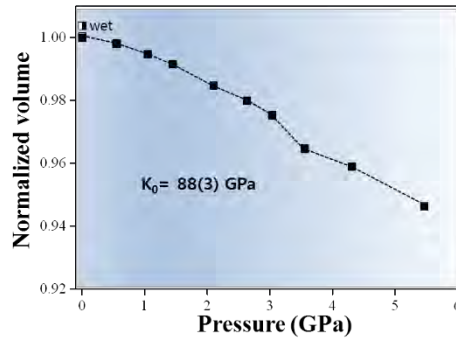
531

532

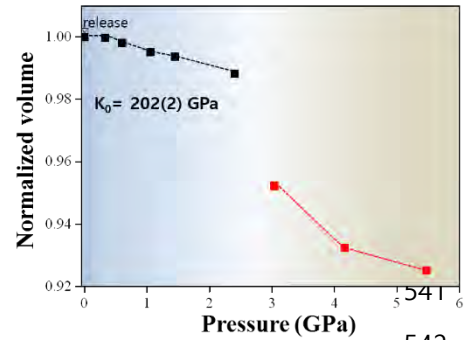
533

534

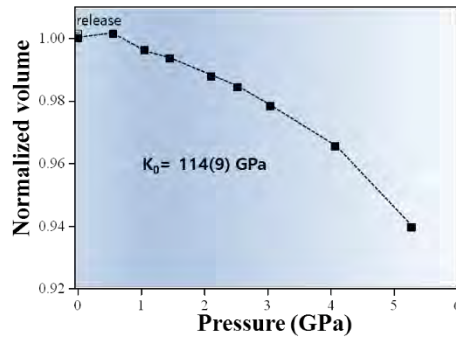
(a) ORI-CHA



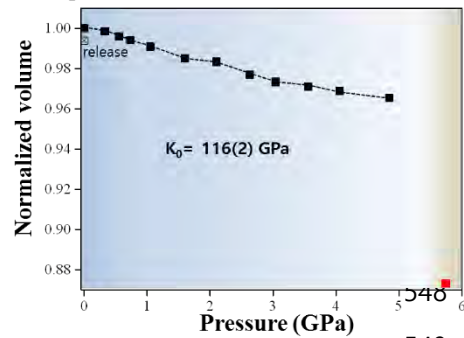
(b) Li-CHA



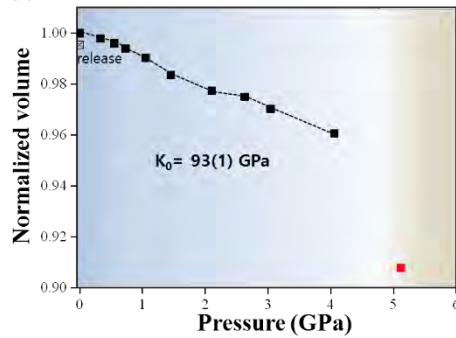
(c) Na-CHA



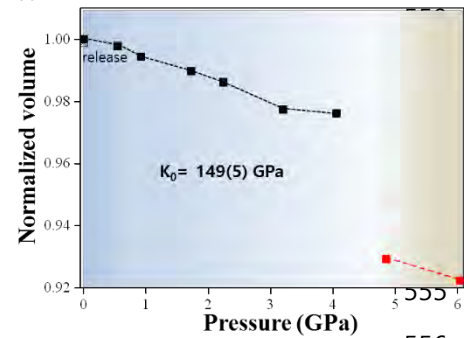
(d) Ag-CHA



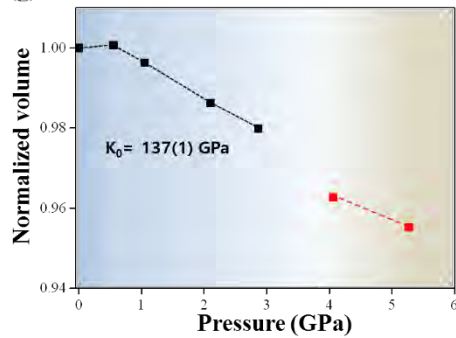
(e) K-CHA



(f) Rb-CHA



(g) Cs-CHA



535

542

549

556

557

558

559

560

561

562

563

564

565

566

567



568 Figure 3.

569

570

571

572

573

574

575

576

577

578

579

580

581

582

583

584

585

586

587

588

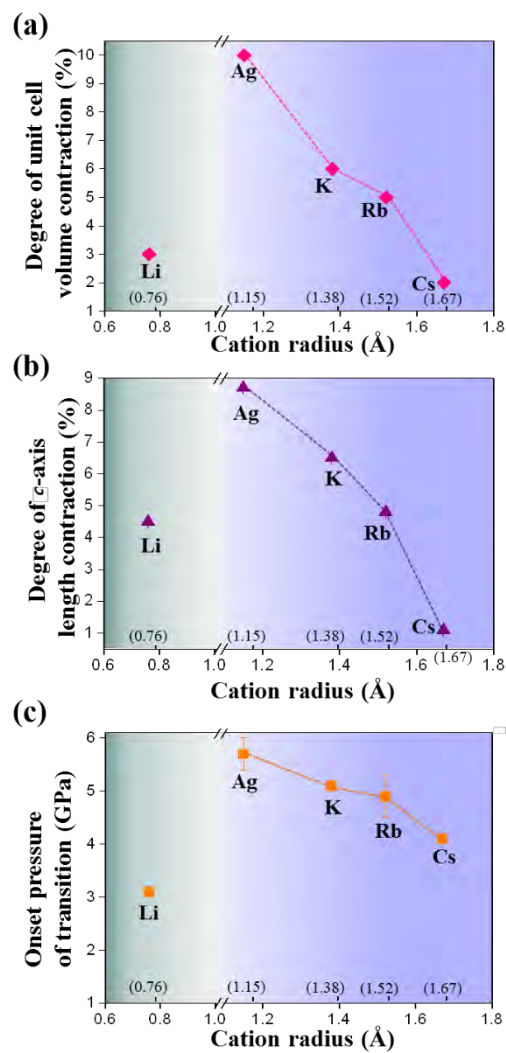
589

590

591

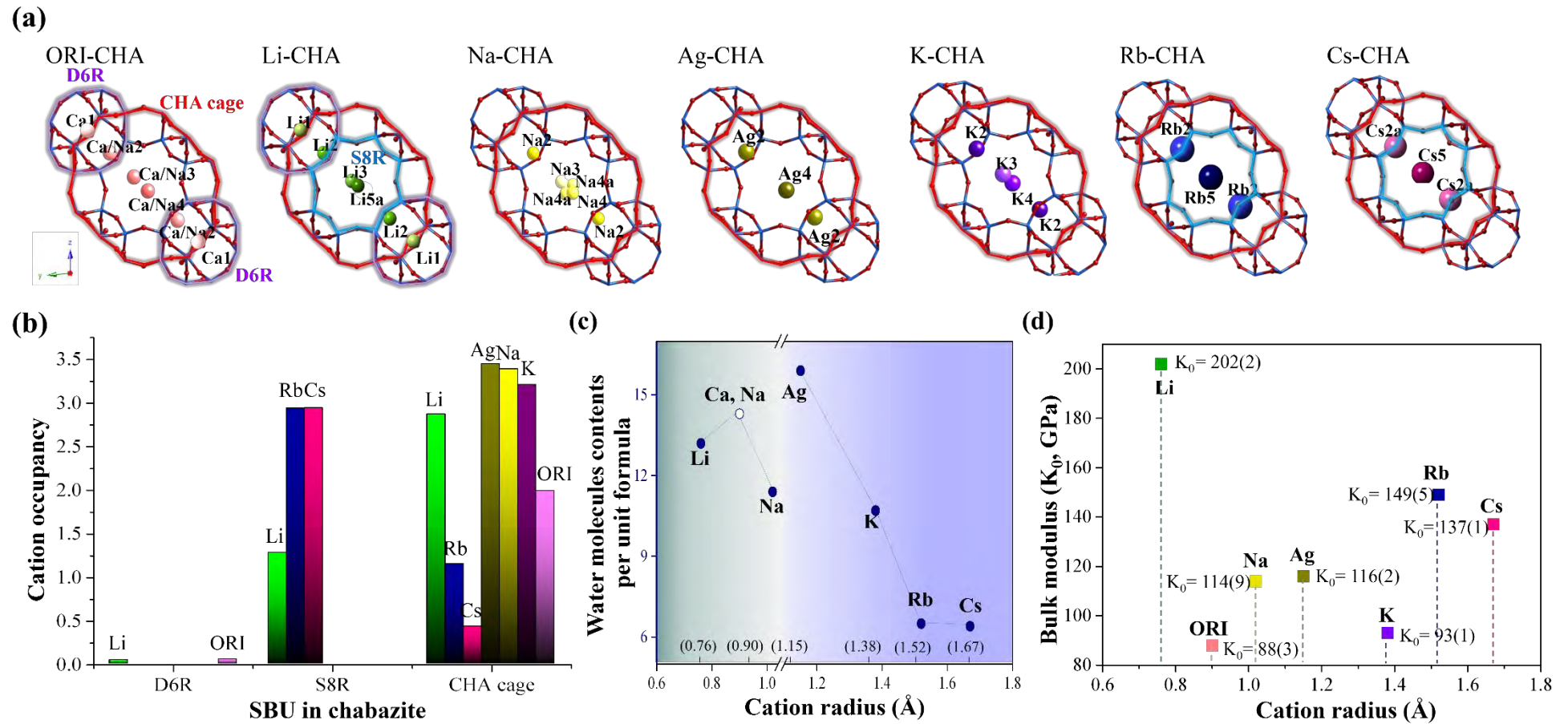
592

593



594 Figure 4.

595



596 Table 1. Changes in the unit-cell edge lengths and volume of the cation-exchanged chabazites  
 597 with *P*, compressed in pure water as pore-penetrating pressure transmitting medium.

ORI-CHA	Ambient	0.55(1) GPa	1.05(1) GPa	1.45(1) GPa	2.10(1) GPa	2.63(1) GPa	3.04(1) GPa	3.56(1) GPa	4.31(1) GPa	5.47(1) GPa	Released
	S.G.	$R\bar{3}m$	$R\bar{3}m$	$R\bar{3}m$	$R\bar{3}m$	$R\bar{3}m$	$R\bar{3}m$	$R\bar{3}m$	$R\bar{3}m$	$R\bar{3}m$	$R\bar{3}m$
$R_{vp}(\%)$	1.56	1.80	1.52	1.71	2.1	1.92	1.58	1.63	1.42	1.53	1.78
$\chi^2$	0.12	0.14	0.10	0.13	0.15	0.14	0.10	0.11	0.10	0.10	0.14
<i>a</i> (Å)	9.405(5)	9.398(8)	9.386(6)	9.375(5)	9.353(3)	9.337(7)	9.332(2)	9.289(9)	9.269(1)	9.228(1)	9.406(6)
$\alpha$ (°)	94.22(2)	94.13(3)	94.02(2)	93.93(3)	93.85(5)	93.83(3)	93.83(3)	93.88(1)	93.73(1)	93.76(2)	94.21(1)
<i>V</i> (Å <sup>3</sup> )	824.9(9)	823.3(3)	820.5(5)	817.8(8)	812.3(3)	808.4(4)	804.4(1)	795.7(1)	791.0(4)	780.6(3)	825.1(1)
Na-CHA	Ambient	0.51(1) GPa	1.01(1) GPa	1.55(1) GPa	2.12(1) GPa	2.52(1) GPa	3.06(1) GPa		4.06(1) GPa	5.27(1) GPa	Released
	S.G.	$R\bar{3}m$	$R\bar{3}m$	$R\bar{3}m$	$R\bar{3}m$	$R\bar{3}m$	$R\bar{3}m$	$R\bar{3}m$	$R\bar{3}m$	$R\bar{3}m$	$R\bar{3}m$
$R_{vp}(\%)$	1.84	1.30	1.56	1.35	2.00	1.8	1.79		1.33	1.25	1.40
$\chi^2$	0.16	0.10	0.10	0.10	0.15	0.12	0.12		0.10	0.10	0.10
<i>a</i> (Å)	9.405(5)	9.409(1)	9.392(1)	9.385(5)	9.367(1)	9.356(1)	9.338(1)		9.298(8)	9.213(2)	9.412(2)
$\alpha$ (°)	94.21(1)	94.14(1)	94.09(1)	94.17(1)	94.19(1)	94.22(1)	94.25(1)		94.32(1)	94.28(4)	94.32(1)
<i>V</i> (Å <sup>3</sup> )	824.9(9)	826.1(1)	821.8(1)	819.7(1)	814.9(1)	812.1(1)	807.2(1)		796.6(1)	775.2(4)	826.2(1)
Ag-CHA	Ambient	0.55(1) GPa	1.03(1) GPa	1.68(1) GPa	1.99(1) GPa	2.63(1) GPa	2.99(1) GPa	3.45(1) GPa	4.85(1) GPa	5.74(1) GPa	Released
	S.G.	$R\bar{3}m$	$R\bar{3}m$	$R\bar{3}m$	$R\bar{3}m$	$R\bar{3}m$	$R\bar{3}m$	$R\bar{3}m$	$R\bar{3}m$	$R\bar{3}m$	$P\bar{1}$
$R_{vp}(\%)$	4.11	2.03	2.27	1.75	1.97	2.38	1.74	1.69	1.52	1.06	2.05
$\chi^2$	1.61	0.36	0.45	0.26	0.32	0.47	0.25	0.24	0.19	0.10	0.35
<i>a</i> (Å)	9.421(1)	9.417(7)	9.402(2)	9.385(5)	9.38(8)	9.36(6)	9.349(9)	9.342(2)	9.332(1)	9.382(4)	9.412(2)
<i>b</i> (Å)										9.112(2)	
<i>c</i> (Å)										8.598(2)	
$\alpha$ (°)	94.17(7)	94.21(1)	94.25(5)	94.39(9)	94.4(4)	94.4(4)	94.43(3)	94.45(5)	94.51(1)	86.29(3)	94.31(1)
$\beta$ (°)										93.00(2)	
$\gamma$ (°)										97.77(2)	
<i>V</i> (Å <sup>3</sup> )	829.2(2)	828.1(1)	823.9(1)	819.1(1)	817.6(6)	812.3(1)	809.3(1)	807.4(1)	804.6(3)	726.0(3)	826.4(1)
Li-CHA	Ambient	0.61(1) GPa	0.98(1) GPa	1.47(1) GPa	2.26(1) GPa		3.06(1) GPa		4.16(1) GPa	5.48(1) GPa	Released
	S.G.	$R\bar{3}m$	$R\bar{3}m$	$R\bar{3}m$	$R\bar{3}m$	$R\bar{3}m$	$P\bar{1}$		$P\bar{1}$	$P\bar{1}$	$R\bar{3}m$
$R_{vp}(\%)$	3.11	2.92	2.84	2.35	3.53		3.41		3.27	2.03	3.49
$\chi^2$	0.47	0.38	0.36	0.24	0.55		0.46		0.43	0.19	0.55
<i>a</i> (Å)	9.396(6)	9.389(9)	9.38(8)	9.374(4)	9.359(9)		9.317(1)		9.307(3)	9.242(2)	9.399(2)
<i>b</i> (Å)							9.299(2)		9.273(2)	9.319(3)	
<i>c</i> (Å)							9.067(2)		8.924(2)	8.881(6)	
$\alpha$ (°)	94.88(8)	94.86(6)	94.86(6)	94.75(5)	94.89(9)		91.00(3)		90.60(3)	91.79(4)	94.8(8)
$\beta$ (°)							92.48(1)		92.47(4)	92.46(5)	
$\gamma$ (°)							95.72(2)		96.53(2)	96.61(3)	
<i>V</i> (Å <sup>3</sup> )	819.9(9)	818.3(1)	815.9(1)	814.6(6)	810.2(1)		780.7(3)		764.4(2)	758.5(5)	821.1(1)
K-CHA	Ambient	0.49(1) GPa	1.00(1) GPa	1.49(1) GPa	2.13(1) GPa	2.62(1) GPa	3.00(1) GPa		4.01(1) GPa	5.12(1) GPa	Released
	S.G.	$R\bar{3}m$	$R\bar{3}m$	$R\bar{3}m$	$R\bar{3}m$	$R\bar{3}m$	$R\bar{3}m$	$R\bar{3}m$	$R\bar{3}m$	$P\bar{1}$	$R\bar{3}m$
$R_{vp}(\%)$	2.63	3.52	3.76	4.01	3.32	3.40	3.41		2.81	2.44	3.91
$\chi^2$	0.36	0.62	0.73	0.81	0.51	0.55	0.57		0.37	0.27	0.73
<i>a</i> (Å)	9.43(3)	9.425(5)	9.405(5)	9.384(4)	9.363(3)	9.355(5)	9.34(4)		9.307(1)	9.285(1)	9.427(7)
<i>b</i> (Å)										9.291(3)	
<i>c</i> (Å)										8.816(2)	
$\alpha$ (°)	94.39(9)	93.97(7)	93.85(5)	93.86(6)	93.8(8)	93.74(4)	93.71(1)		93.59(1)	90.77(3)	94.3(3)
$\beta$ (°)										93.95(2)	
$\gamma$ (°)										93.47(2)	
<i>V</i> (Å <sup>3</sup> )	830.8(8)	830.8(8)	826.1(1)	820.5(5)	815.3(1)	813.3(1)	809.4(1)		801.4(2)	757.3(2)	830.3(3)
Rb-CHA	Ambient	0.51(1) GPa	0.92(1) GPa	1.73(1) GPa	2.24(1) GPa		3.20(1) GPa	3.96(1) GPa	4.87(1) GPa	6.04(1) GPa	Released
	S.G.	$R\bar{3}m$	$R\bar{3}m$	$R\bar{3}m$	$R\bar{3}m$	$R\bar{3}m$	$R\bar{3}m$	$R\bar{3}m$	$P\bar{1}$	$P\bar{1}$	$R\bar{3}m$

$R_{wp}^2$ (%)	1.84	2.54	2.36	2.16	1.56	2.11	1.52	2.02	1.87	4.88
$\chi^2$	0.47	0.50	0.44	0.36	0.18	0.34	0.17	0.32	0.26	1.84
$a$ (Å)	9.416(6)	9.417(7)	9.406(6)	9.39(9)	9.379(9)	9.352(2)	9.35(5)	9.24(4)	9.218(2)	9.416(1)
$b$ (Å)								9.352(3)	9.342(4)	
$c$ (Å)								8.967(2)	8.933(5)	
$\alpha$ (°)	94.69(9)	94.45(5)	94.42(2)	94.36(6)	94.36(6)	94.42(2)	94.56(1)	91.51(2)	91.9(9)	94.58(1)
$\beta$ (°)								92.72(2)	92.86(4)	
$\gamma$ (°)								95.01(2)	95.3(3)	
$V$ (Å <sup>3</sup> )	826.0(1)	827.2(2)	824.3(3)	820.5(1)	817.5(5)	810.2(1)	809.2(3)	770.2(2)	764.5(4)	826.4(2)
<b>Cs-CHA</b>	Ambient	0.45(1) GPa	0.98(1) GPa		2.15(1) GPa	2.87(1) GPa		4.09(1) GPa	5.24(1) GPa	Released
S.G.	$R\bar{3}m$	$R\bar{3}m$	$R\bar{3}m$		$R\bar{3}m$	$R\bar{3}m$		$P\bar{1}$	$P\bar{1}$	$R\bar{3}m$
$R_{wp}^2$ (%)	2.23	3.44	5.00		3.49	3.57		1.96	1.87	3.52
$\chi^2$	0.25	0.58	1.23		0.57	0.57		0.17	0.16	0.58
$a$ (Å)	9.427(7)	9.429(9)	9.415(5)		9.383(3)	9.363(3)		9.296(2)	9.269(1)	9.427(1)
$b$ (Å)								9.313(1)	9.261(2)	
$c$ (Å)								9.324(1)	9.328(1)	
$\alpha$ (°)	94.25(5)	94.26(6)	94.26(6)		94.21(1)	94.22(2)		94.53(1)	94.78(1)	94.24(4)
$\beta$ (°)								95.27(1)	95.19(2)	
$\gamma$ (°)								93.5(5)	92.96(2)	
$V$ (Å <sup>3</sup> )	830.4(4)	831.0(1)	827.3(3)		819.1(1)	813.7(1)		799.4(2)	793.2(2)	830.5(1)

598